NANO LETTERS

pubs.acs.org/NanoLett Letter

Signatures of Three-State Potts Nematicity in Spin Excitations of the van der Waals Antiferromagnet $FePSe_3$

Weiliang Yao,* Viviane Peçanha-Antonio, Devashibhai T. Adroja, Steven J. Gomez Alvarado, Bin Gao, Sijie Xu, Ruixian Liu, Xingye Lu,* and Pengcheng Dai*

Cite This: https://doi.org/10.1021/acs.nanolett.5c06293 Read Online

ACCESS | Metrics & More | Article Recommendations | Supporting Information

ABSTRACT: In two-dimensional (2D) nearly square-lattice quantum materials, electron correlations can induce an electronic nematic phase with 2-fold rotational (C_2) symmetry. For 2D materials with 3-fold rotational (C_3) symmetry, such as the honeycomb lattice, a vestigial three-state Potts nematic order has been observed in the van der Waals antiferromagnet $FePSe_3$ under uniaxial strain. Here, we use neutron scattering to probe the magnetic order and spin excitations of $FePSe_3$ under uniaxial strain. In the antiferromagnetic (AFM) ordered state, ~0.6% tensile strain suppresses one zigzag domain and enhances the other two, reducing the AFM order and spin waves to C_2 symmetry. This broken C_3 symmetry in spin excitations persists slightly above $T_N \approx 108.6$ K, where zigzag AFM order is absent. These results provide direct evidence of magnetoelastic coupling and suggest that three-state Potts nematicity in paramagnetic spin excitations originates as the vestigial order of the low-temperature zigzag AFM state.

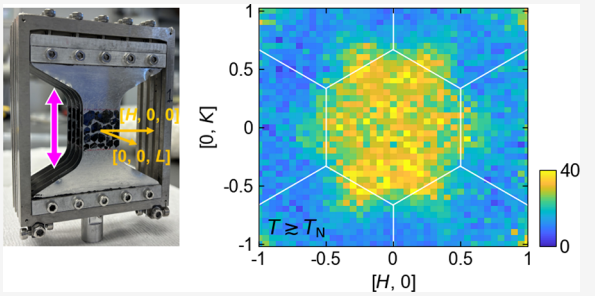

KEYWORDS: *van der Waals antiferromagnets, spin excitations, nematic order, uniaxial strain*

Symmetry breaking, such as the formation of new magnetic, structural, or electronic orders, is a fundamental phenomenon in nature. Understanding the nature of symmetry breaking can provide crucial insights into the underlying laws that govern the physical properties of materials.[1] In periodic crystalline solids, rotational symmetry refers to the property that the material remains invariant under rotation by a specific angle. Owing to translational symmetry, crystalline solids can only host 2-fold, 3-fold, 4-fold, or 6-fold discrete rotational symmetries, denoted as C_2, C_3, C_4, and C_6, respectively.[2]

A nematic phase originates from a state where elongated molecules in liquid crystals exhibit no crystalline positional order but are aligned with their long axes approximately parallel, forming directional order with C_2 symmetry.[3] In liquid crystals, it is an intermediate phase between an ordered crystalline solid and a disordered liquid.[3] An electronic nematic phase, predicted to occur in a two-dimensional (2D) square-lattice Mott insulator,[4] typically breaks the C_4 symmetry of the underlying lattice and arises near a superconducting phase.[5−9] Since its discovery in copper- and iron-based high-temperature superconductors with nearly square-lattice structures,[10,11] studies of nematicity have often focused on the spontaneous reduction of C_4 symmetry to C_2 in transport, electronic, and magnetic properties, implying that the system selects one of two energetically equivalent configurations (Ising nematicity).[5−9]

For crystalline solids with C_3 or C_6 symmetry,[12] it is also possible to develop a nematic state that selects one (or two) out of three equivalent configurations—a phenomenon known as three-state Potts nematicity.[13−15] Materials in the hexagonal crystal family are thus an ideal platform to explore this type of symmetry breaking. Recent studies on systems with triangular, kagome, and honeycomb lattices have reported intriguing nematic behaviors in their electronic and/or magnetic properties, including $Fe_{1/3}NbS_2$,[16] $Co_{1/3}TaS_2$,[17,18] CsV_3Sb_5,[19−21] ScV_6Sn_6,[22] $FePSe_3$,[23,24] and $NiPS_3$.[25] However, studies to date have used optical, transport, or thermodynamic methods, which cannot directly probe the microscopic origin of the C_3 symmetry breaking in the nematic regime or determine the energy scale of the corresponding nematic fluctuations.

In this work, we focus on the van der Waals antiferromagnet $FePSe_3$, which crystallizes in a rhombohedral $R\bar{3}$ structure consisting of hexagonal layers stacked along the c-axis through weak van der Waals interactions [Figure 1(a)].[26,27] The Fe ions, with localized magnetic moments, form a honeycomb lattice [Figure 1(b)] that develops long-range antiferromagnetic (AFM) order below $T_N \approx 108$ K.[23,24,28,29] Neutron diffraction experiments identified a zigzag magnetic structure

Received: December 16, 2025
Revised: February 19, 2026
Accepted: February 20, 2026

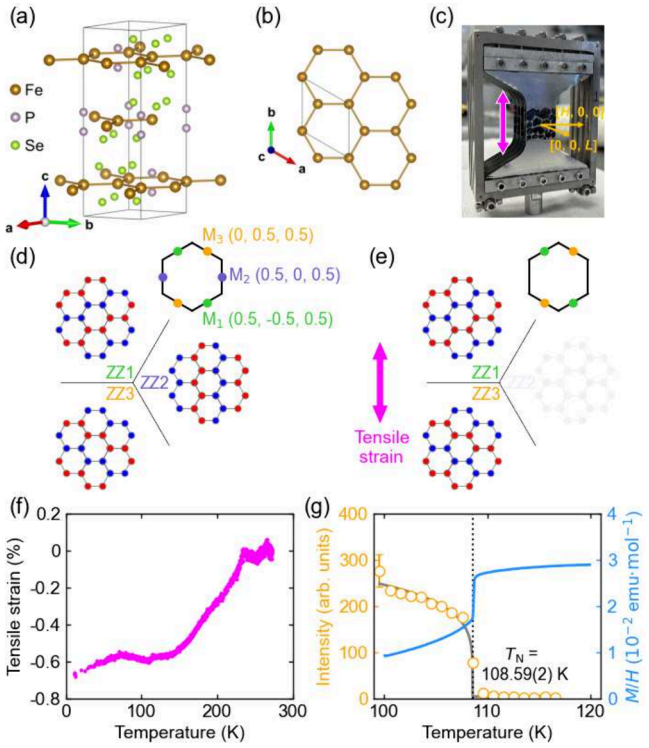

Figure 1. (a) Crystal structure of $FePSe_3$. (b) Honeycomb lattice formed by Fe ions. (c) Strain device with $FePSe_3$ single crystals attached. The magenta double arrow indicates the tensile strain direction. (d) Three zigzag domains (ZZ1, ZZ2, and ZZ3) in the unstrained Fe honeycomb lattice, where red and blue represent spins pointing into and out of the honeycomb plane. The inset (upper right) shows the six magnetic Bragg peaks in the hexagonal Brillouin zone corresponding to the three zigzag domains. (e) Two remaining zigzag domains (ZZ1 and ZZ3) under tensile strain. (f) Temperature dependence of the tensile strain applied to $FePSe_3$ single crystals.[33] (g) Temperature dependence of the diffraction intensity at Bragg peak (0, 0.5, 0.5) (left axis) and the magnetic susceptibility under a 0.5 T *c*-axis field (right axis). The gray solid curve is a power-law fit to the diffraction data, as described in the text. The dashed vertical line marks T_N.

with propagation wave vector $\mathbf{k}_m$ = (0.5, 0, 0.5) and revealed the weakly first-order nature of the AFM transition, consistent with heat-capacity measurements.[30−32] Due to the intrinsic C_3 symmetry of the honeycomb lattice, there are three possible zigzag domains [ZZ1, ZZ2, and ZZ3 in Figure 1(d)]. In neutron diffraction, ZZ1, ZZ2, and ZZ3 domains contribute to magnetic Bragg peaks at the three *M*-points of the hexagonal Brillouin zone [M_1, M_2, and M_3 in the inset of Figure 1(d)]. Therefore, one can use the Bragg peak intensities to directly monitor the populations of these zigzag domains.

Recent optical linear dichroism (LD) and elastocaloric measurements have revealed a novel nematic state in $FePSe_3$, in which the C_3 lattice symmetry gives rise to a three-state Potts nematicity associated with the underlying AFM order.[23,24] Without externally applied uniaxial strain, the three equally populated zigzag domains below T_N constitute a three-state Potts state. In-situ uniaxial strain was used to tune this three-state Potts state and extract the corresponding susceptibility, which exhibits divergent behavior near T_N, indicating the formation of a three-state Potts nematic state.[23] Since $FePSe_3$ is an AFM insulator, the nematicity is solely related to the spin degrees of freedom. $FePSe_3$ therefore offers a unique opportunity to study the physics of three-state Potts nematicity arising from spin interactions. While LD and elastocaloric measurements can provide useful information on the three-state Potts nematic regime, they are not microscopic probes and thus cannot unveil the wave vector of the magnetic order or the momentum dependence of the spin dynamics in the nematic state. In copper- and iron-based high-temperature superconductors,[10,35] anisotropic spin excitations in momentum space detected by inelastic neutron scattering (INS) experiments provided direct proof of the nematic state and its connection with anisotropic transport and electronic properties.[6−9]

To study possible nematic spin excitations in $FePSe_3$, we conducted INS experiments on $FePSe_3$ single crystals under the application of uniaxial strain, which allows direct control over the populations of different zigzag domains. For a magnet with a strongly first-order AFM transition, critical spin fluctuations around T_N are typically absent, resulting in no or only weak nematic behavior. In contrast, for a weakly first-order AFM transition, uniaxial strain can enhance critical spin fluctuations near the AFM transition regime, thereby promoting a nematic phase (regime), as observed in weakly first-order AFM $BaFe_2As_2$[36−38] and strongly first-order AFM $SrFe_2As_2$.[39] In the case of unstrained $FePSe_3$, the weakly first-order nature of the AFM transition[30,32] suggests that static magnetic order and spin excitations should obey C_3 symmetry, consistent with the underlying honeycomb lattice. However, when uniaxial strain detwins the three magnetic domains, C_2-symmetric diffraction and spin-wave patterns are expected below T_N. When the system is warmed above T_N with suppressed static magnetic order, the spin excitations should become gapless immediately with the C_3 symmetry if there are no critical spin fluctuations or a nematic regime. Conversely, if the restoration of the C_3 symmetry is delayed until several K above T_N, the C_2-symmetric spin excitations in the paramagnetic state would be a signature of the underlying three-state Potts nematicity appearing at temperatures above T_N.

We utilized a novel uniaxial strain device previously used to detwin FeSe single crystals, in which thin aluminum plates are mounted onto the invar alloy frames to induce weakly temperature-dependent uniaxial tensile strain.[40] About 1 g of $FePSe_3$ single crystals were coaligned and attached to the thin aluminum plates of the strain device, with the crystallographic (*H*, 0, *L*) plane placed in the horizontal scattering plane [Figure 1(c)]. When cooling down to below 150 K, a uniaxial tensile strain of about 0.6% is applied along the [−0.5*K*, *K*, 0] direction (i.e., perpendicular to the nearest Fe−Fe bond) [Figure 1(f)], which was determined by in situ strain-gauge measurements.[33,41] Our INS experiment using this strain device was conducted on the time-of-flight spectrometer MERLIN[42] at the ISIS neutron and muon source, Rutherford Appleton Laboratory, UK. More details of the experiment and data analysis can be found in.[41]

Figure 1(g) presents the temperature dependence of the intensity at the magnetic Bragg peak M_2 (0, 0.5, 0.5) under uniaxial strain, which shows a typical order-parameter behavior. By fitting the data with a power-law function $I = A(T - T_N)^{2\beta} + B$ (A and B are the scale and background constants, respectively, and β is the critical exponent of the order parameter), we find T_N = 108.59(2) K and β = 0.10(1). The obtained T_N coincides with the sharp magnetic susceptibility anomaly in the unstrained case [Figure 1(g)],

https://doi.org/10.1021/acs.nanolett.5c06293
Nano Lett. XXXX, XXX, XXX−XXX

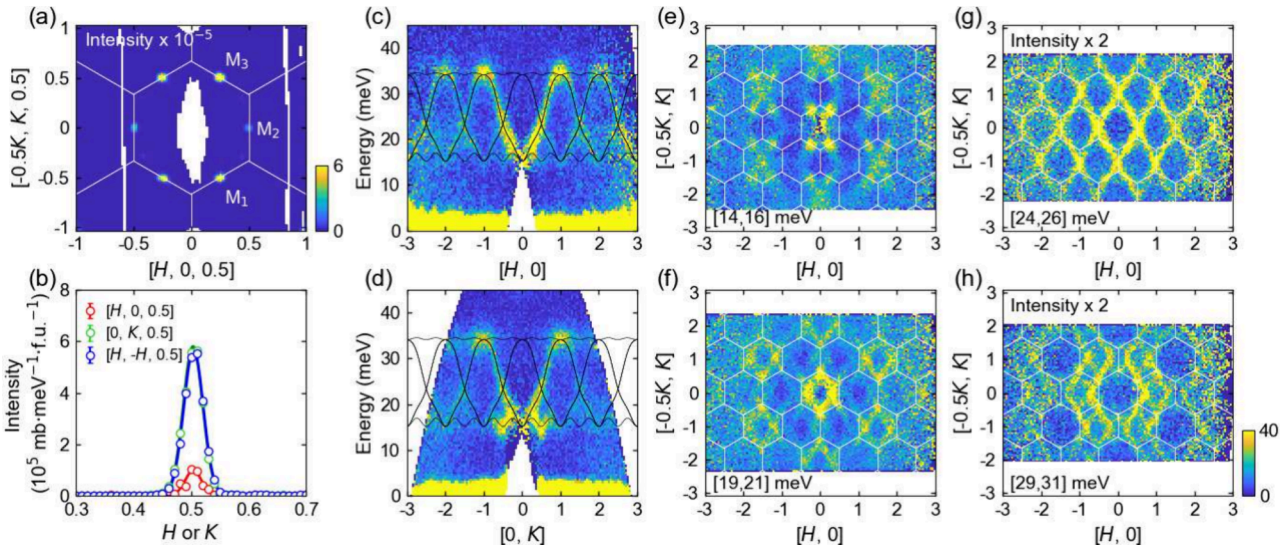

Figure 2. (a) Elastic scattering pattern of the (H, K, 0.5) plane at 6.0 K. White solid lines mark Brillouin zone boundaries. f.u.: formula unit. (b) Momentum dependence of the intensities around three magnetic Bragg peaks [M_2, M_3, and M_1 in the inset of Figure 1(d) and (e)] along [H, 0, 0.5], [0, K, 0.5], and [H, −H, 0.5]. Solid curves are Gaussian fits. (c, d) Magnetic excitation spectra along [H, 0] and [0, K] at 6.0 K. Black solid curves are calculated spin-wave dispersions using SpinW.[34] (e−h) Constant-energy slices of the spectra around 15, 20, 25, and 30 meV at 6.0 K.

which confirms that the transition temperature is unchanged by the uniaxial strain. However, the critical exponent becomes closer to the limit of the 2D Ising model (β = 1/8),[30] suggesting the magnetic phase transition approaches second order under uniaxial strain, similar to previous works on $BaFe_2As_2$.[36−38]

A diffraction pattern of the (H, K, 0.5) plane at 6.0 K is shown in Figure 2(a), from which we find that M_1 and M_3 basically have the same intensity while M_2 is much weaker. Since our sample consists of many coaligned single crystals [Figure 1(c)],[41] we expect the three zigzag domains to be present in equal quantities without the strain.[30] Our observation thus suggests that the ZZ2 domain is strongly suppressed by the uniaxial strain, and the ZZ1 and ZZ3 domains are favored [see Figure 1(e)]. Such strain control of the zigzag domains is consistent with previous reports based on optical methods.[23,24] By extracting the integrated Bragg peak intensities of M_1, M_2, and M_3 (I_{M1}, I_{M2}, and I_{M3}) [Figure 2(b)], we estimate a detwinning ratio of $\eta = \frac{(I_{M1}+I_{M3})/2 - I_{M2}}{(I_{M1}+I_{M3})/2 + I_{M2}} \approx 75.7\%$, which is comparable with the experiment on FeSe.[40]

Next, we turn to the strain effect on the magnetic excitation spectra. Since $FePSe_3$ is a quasi-2D antiferromagnet with interlayer exchange interactions much weaker than intralayer ones,[30] we integrated over a wide range of L and present the spectra within the honeycomb plane.[41] Spin waves along the [H, 0] and [0, K] directions at 6.0 K are shown in Figure 2(c) and (d), respectively. While the overall dispersions are similar for the two directions, the intensity distributions (dynamic structure factors) exhibit a clear difference. In particular, the low-lying spin-wave branch around 16 meV is strongly suppressed along [H, 0], suggesting that this branch is associated with ZZ2 domain[41] and that low-energy spin excitations are more susceptible to external perturbations. Nevertheless, the measured dispersions can still be well described by previously determined parameters within linear spin-wave theory [Figure 2(c) and (d)],[30] indicating that the exchange interactions remain essentially unchanged under ~0.6% tensile strain and that zigzag domain repopulation is the dominant effect. Constant-energy slices in Figure 2(e)−(h) further demonstrate that the system exhibits C_2 symmetry at low temperature, consistent with the pronounced optical LD signals.[23,24]

On warming to 108.8 K, which is slightly above T_N, sharp spin waves completely disappear and the broad excitations shift to lower energies [Figure 3(a) and (b)]. Despite very similar spectra along the [H, 0] and [0, K] directions, spin excitations along the [H, 0] direction are overall broader than those along the [0, K] direction. Figure 3(c) and (d) presents the constant-energy slices taken around 8 and 12 meV, respectively. While the intensity distribution in the hexagonal Brillouin zone shows nearly C_3 symmetry around 8 meV, violation of it is evident for the pattern around 12 meV, which is C_2-symmetric about the c-axis. The breaking of the C_3 symmetry can be more clearly seen from the momentum dependence of the intensity, as shown in Figure 3(e) and (f). Around 12 meV, the intensities along the [0, K] and [H, −H] directions are essentially the same, but they deviate from those along the [H, 0] direction near the M points of the Brillouin zone [H or K = 0.5 in Figure 3(f)] by approximately 10 mb·meV^{-1}·f.u.$^{-1}$. These observations suggest the spin fluctuations of $FePSe_3$ show nematicity without the presence of long-range magnetic order.

The C_3 symmetry of the spin excitation spectrum is gradually restored at higher temperatures (109.5 and 113.0 K), as can be seen in Figure 4(a)−(d). To show the evolution of the C_3 symmetry breaking (or nematicity) above T_N, we use the intensity difference $\Delta I(\mathbf{Q})$, which is defined as $\Delta I(\mathbf{Q}) = [I_1(\mathbf{Q}) + I_3(\mathbf{Q})]/2 - I_2(\mathbf{Q})$, where $I_1(\mathbf{Q})$, $I_2(\mathbf{Q})$, and $I_3(\mathbf{Q})$ are the intensity distributions along the paths 1, 2, and 3 shown in Figure 3(c). We note that, for strictly C_3-symmetric spin excitations, $\Delta I(\mathbf{Q}) = 0$. Therefore, this quantity can measure the C_3 symmetry breaking and may be regarded as an effective nematic order parameter.[5] The $\Delta I(\mathbf{Q})$ at three temperatures is presented in Figure 4(e), where it is nonzero at 108.8 and 109.5 K, and finally dies away at 113.0 K. In comparison, the spin excitation spectrum consistently exhibits C_3 symmetry both above and below T_N without the uniaxial strain.[30] The

https://doi.org/10.1021/acs.nanolett.5c06293
Nano Lett. XXXX, XXX, XXX−XXX

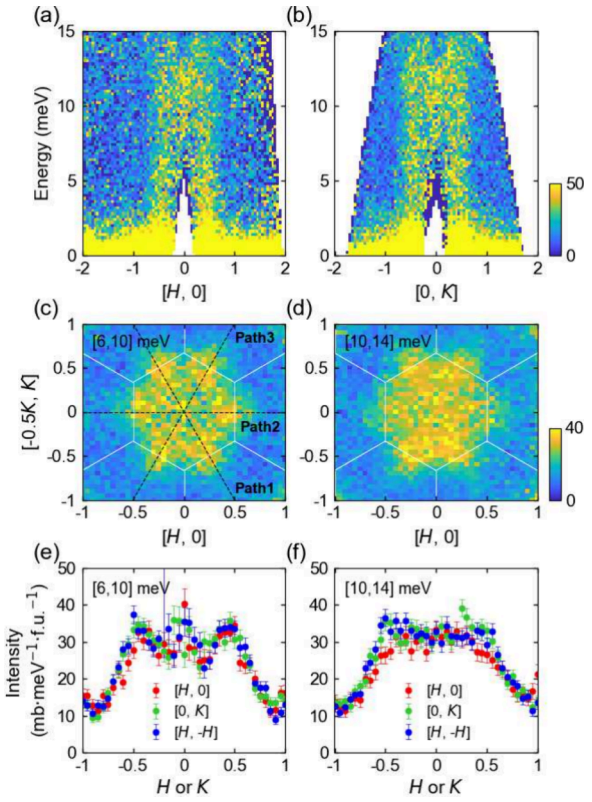

Figure 3. (a, b) Spin excitation spectra along $[H, 0]$ and $[0, K]$ at 108.8 K. (c, d) Constant-energy slices of the excitation spectra around 8 and 12 meV at 108.8 K. (e, f) Momentum dependence of the intensities around 8 and 12 meV along $[H, 0]$, $[0, K]$, and $[H, -H]$ [paths 2, 3, and 1 in (c), respectively].

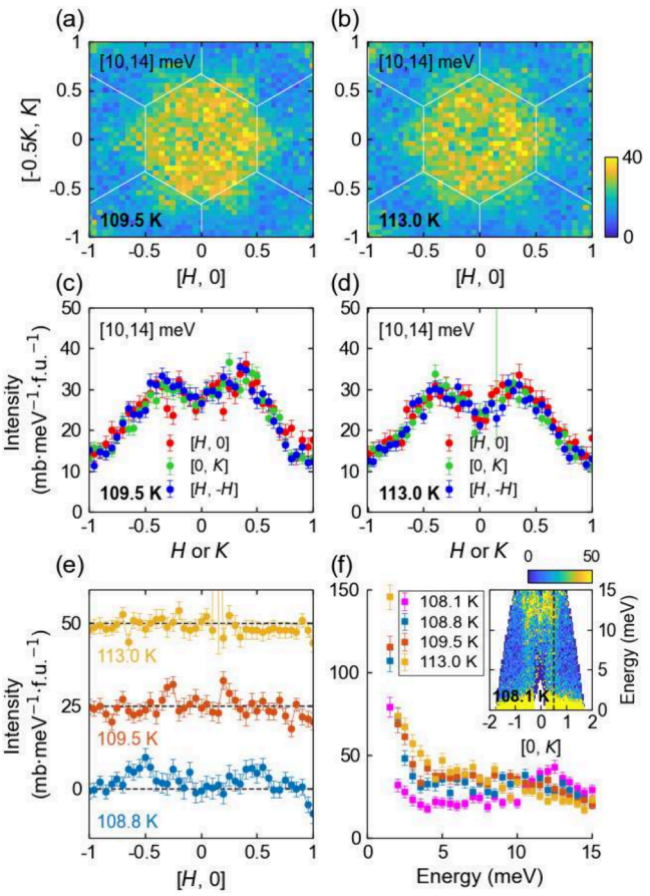

Figure 4. (a, b) Constant-energy slices of the spin excitation spectra around 12 meV at 109.5 and 113.0 K. (c, d) Momentum dependence of the intensities around 12 meV along $[H, 0]$, $[0, K]$, and $[H, -H]$ at 109.5 and 113.0 K. (e) Momentum dependence of the intensity difference (see text) around 12 meV. Data from different temperatures are evenly offset for clarity. Horizontal dashed lines indicate zero intensity for each temperature. (f) Energy dependence of the intensities around (0, 0.5) at 108.1, 108.8, 109.5, and 113.0 K. Inset shows the spin excitation spectrum along $[0, K]$ at 108.1 K. The vertical dashed line marks (0, 0.5).

complete disappearance of the C_3 symmetry breaking at 113.0 K also suggests that the feature observed at lower temperatures is not simply due to the applied strain (e.g., mechanical effects) but is intrinsic to the magnetic response. Otherwise, the spectrum at 113.0 K will also show the same anisotropy since the applied strain is almost in the same level [see Figure 1(f)]. The quick decay of the nematic signal above T_N is consistent with the hyperbola behavior (with respect to temperature) of the nematic susceptibility determined previously.[23] With increasing strain, the AFM transition becomes more second-order-like, thus increasing the critical regime as shown in.[23] For the level of strain we applied (~0.6%), the nematic and AFM transition temperatures are expected to nearly merge together,[23] thus giving rise to the narrow temperature regime above T_N where the C_3-symmetry-breaking spin excitations are observed.

To further check the characteristics of the spin excitations near T_N, we show the energy dependence of the intensity at (0, 0.5) in Figure 4(f). At 108.1 K (slightly below T_N), an energy gap of ~13 meV can be resolved, signifying the Ising anisotropy of the spin waves [see also in the inset of Figure 4(f)]. However, the energy gap fully closes at 108.8 K and above. This suggests the nematic spin excitations we observed are in the paramagnetic state, which differs from the anisotropic spin waves below T_N due to the detwinning of zigzag domains. Therefore, the nematic spin excitations slightly above T_N, a hallmark of the three-state Potts nematic state, are a vestigial order for the zigzag AFM order below T_N, and likely arise from a strain-induced nematic regime similar to iron pnictides.[6−9] As in studies of nematicity in other quantum materials, uniaxial strain is required here to reveal the nematic behavior, since the C_3-symmetric honeycomb lattice would otherwise smear out the intrinsic C_2 symmetry at the macroscopic level.

Our experimental results unveil the following sequences of the magnetic phases in $FePSe_3$. On cooling from the high-temperature paramagnetic spin-disordered state, the system first enters the uniaxial strain-induced three-state Potts nematic state, where the spin excitations are still highly fluctuating but show anisotropy in reciprocal space due to spin−lattice coupling. In the absence of external strain, the nematic order exhibits equal probability along the three equivalent directions of the honeycomb lattice, which hence leads to the C_3-symmetric excitation patterns as observed previously.[30] When the external strain is applied to induce a tiny lattice distortion, it disfavors the nematic director perpendicular to the strain direction.[23,24] Due to the divergent nature of the nematic susceptibility, the strain effect is most pronounced close to T_N,[23] which results in the C_2-symmetric excitation pattern. At temperatures lower than T_N, the long-range zigzag AFM order condenses mainly around the M-points where the nematic

https://doi.org/10.1021/acs.nanolett.5c06293
Nano Lett. XXXX, XXX, XXX−XXX

fluctuations are most significant, and finally establishes the two preferred zigzag domains of dominant population.

The nematic spin excitations observed in $FePSe_3$ are reminiscent of those in iron-based superconductors such as $BaFe_{2-x}Ni_xAs_2$[35] and FeSe.[40,43] In these systems, the C_4 symmetry of the paramagnetic spin excitations becomes C_2 symmetry in the magnetic ordered state due to orthorhombic lattice distortion and collinear AFM order along the *a*-axis of the orthorhombic lattice.[8] On warming to the paramagnetic tetragonal state slightly above T_N, spin excitations are C_4-symmetric without uniaxial strain. However, when a uniaxial strain is applied along one of the tetragonal axis, the low-energy spin excitations become anisotropic along the $[H, 0]$ and $[0, K]$ directions in the 2D square Brillouin zone over a broad range above T_N, forming a strain-driven nematic phase.[35,40,43] In contrast, the uniaxial strain induced spin excitation anisotropy in $FePSe_3$ form in an extremely narrow regime above T_N before becoming isotropic in reciprocal space. This is most likely due to the fact that the AFM phase transition under uniaxial strain is still first-order-like with a narrow critical temperature regime and weak critical spin fluctuations. In addition, while the nematic phase in iron-based superconductors is clearly associated with tetragonal-to-orthorhombic lattice distortion,[6−9] there is no known lattice distortion associated with the AFM phase transition in $FePSe_3$,[30,31] suggesting that magnetoelasticity may not drive the order−disorder phase transition.[44] Nevertheless, the fact that a uniaxial tensile strain of about 0.6% induces anisotropy in paramagnetic spin excitations of $FePSe_3$ suggests a small but finite magnetoelastic coupling.

In summary, by performing INS experiments on $FePSe_3$ single crystals under uniaxial tensile strain, we have mapped out the spin excitation spectra and studied their evolution with temperature. Although the applied strain is only about 0.6%, we observed a significant detwinning effect of the zigzag domains in the AFM ordered state and the corresponding spin waves featuring C_2 symmetry. Moreover, in the paramagnetic state just above the ordering temperature, the spin excitations still exhibit broken C_3 symmetry in a narrow temperature regime, suggesting the presence of magnetoelastic coupling and the underlying three-state Potts nematicity in the spin excitation spectra of $FePSe_3$.

■ ASSOCIATED CONTENT

Supporting Information

The Supporting Information is available free of charge at https://pubs.acs.org/doi/10.1021/acs.nanolett.5c06293.

Additional information about characterization of $FePSe_3$ single crystals and additional neutron scattering data (PDF)

■ AUTHOR INFORMATION

Corresponding Authors

Weiliang Yao − *Department of Physics and Astronomy, Rice University, Houston, Texas 77005, United States; Rice Laboratory for Emergent Magnetic Materials and Smalley-Curl Institute, Rice University, Houston, Texas 77005, United States;* orcid.org/0009-0000-7014-1659; Email: wy28@rice.edu

Xingye Lu − *Center for Advanced Quantum Studies, School of Physics and Astronomy, and Key Laboratory of Multiscale Spin Physics (Ministry of Education), Beijing Normal University, Beijing 100875, People's Republic of China*; Email: luxy@bnu.edu.cn

Pengcheng Dai − *Department of Physics and Astronomy, Rice University, Houston, Texas 77005, United States; Rice Laboratory for Emergent Magnetic Materials and Smalley-Curl Institute, Rice University, Houston, Texas 77005, United States*; Email: pdai@rice.edu

Authors

Viviane Peçanha-Antonio − *ISIS Facility, STFC, Rutherford Appleton Laboratory, Didcot, Oxfordshire OX11 0QX, United Kingdom*

Devashibhai T. Adroja − *ISIS Facility, STFC, Rutherford Appleton Laboratory, Didcot, Oxfordshire OX11 0QX, United Kingdom; Highly Correlated Matter Research Group, Physics Department, University of Johannesburg, Auckland Park 2006, South Africa*

Steven J. Gomez Alvarado − *Department of Physics and Astronomy, Rice University, Houston, Texas 77005, United States; Rice Laboratory for Emergent Magnetic Materials and Smalley-Curl Institute, Rice University, Houston, Texas 77005, United States;* orcid.org/0000-0002-5783-1126

Bin Gao − *Department of Physics and Astronomy, Rice University, Houston, Texas 77005, United States; Rice Laboratory for Emergent Magnetic Materials and Smalley-Curl Institute, Rice University, Houston, Texas 77005, United States;* orcid.org/0000-0002-2853-2362

Sijie Xu − *Department of Physics and Astronomy, Rice University, Houston, Texas 77005, United States; Rice Laboratory for Emergent Magnetic Materials and Smalley-Curl Institute, Rice University, Houston, Texas 77005, United States*

Ruixian Liu − *Center for Advanced Quantum Studies and Department of Physics, Beijing Normal University, Beijing 100875, People's Republic of China*

Complete contact information is available at: https://pubs.acs.org/10.1021/acs.nanolett.5c06293

Notes

The authors declare no competing financial interest.

■ ACKNOWLEDGMENTS

The neutron scattering work at Rice is supported by the U.S. NSF DMR-2401084 (P.D.). The single-crystal growth work at Rice is supported by the Robert A. Welch Foundation under grant no. C-1839 (P.D.). X.L. at BNU is supported by the Scientific Research Innovation Capability Support Project for Young Faculty (ZYGXQNJSKYCXNLZCXM-M2). The experiment at the ISIS Neutron and Muon Source was supported by a beam time allocation RB2510117 from the Science and Technology Facilities Council.

■ REFERENCES

(1) Beekman, A. J.; Rademaker, L.; van Wezel, J. An introduction to spontaneous symmetry breaking. *SciPost Phys. Lect. Notes* **2019**, *11*, na.

(2) Ashcroft, N. W.; Mermin, N. D. *Solid State Physics*; Holt-Saunders, New York, 1976.

(3) De Gennes, P.-G.; Prost, J. *The physics of liquid crystals*; Oxford University Press, 1993.

(4) Kivelson, S. A.; Fradkin, E.; Emery, V. J. Electronic liquid-crystal phases of a doped Mott insulator. *Nature* **1998**, *393*, 550−553.

(5) Fradkin, E.; Kivelson, S. A.; Lawler, M. J.; Eisenstein, J. P.; Mackenzie, A. P. Nematic Fermi fluids in condensed matter physics. *Annu. Rev. Condens. Matter Phys.* **2010**, *1*, 153−178.
(6) Fernandes, R. M.; Orth, P. P.; Schmalian, J. Intertwined vestigial order in quantum materials: Nematicity and beyond. *Annual Review of Condensed Matter Physics* **2019**, *10*, 133−154.
(7) Nie, L.; Tarjus, G.; Kivelson, S. A. Quenched disorder and vestigial nematicity in the pseudogap regime of the cuprates. *Proc. Natl. Acad. Sci. U. S. A.* **2014**, *111*, 7980−7985.
(8) Dai, P. Antiferromagnetic order and spin dynamics in iron-based superconductors. *Rev. Mod. Phys.* **2015**, *87*, 855−896.
(9) Böhmer, A. E.; Chu, J.-H.; Lederer, S.; Yi, M. Nematicity and nematic fluctuations in iron-based superconductors. *Nat. Phys.* **2022**, *18*, 1412−1419.
(10) Hinkov, V.; Haug, D.; Fauqué, B.; Bourges, P.; Sidis, Y.; Ivanov, A.; Bernhard, C.; Lin, C. T.; Keimer, B. Electronic Liquid Crystal State in the High-Temperature Superconductor $YBa_2Cu_3O_{6.45}$. *Science* **2008**, *319*, 597−600.
(11) Chu, J.-H.; Analytis, J. G.; De Greve, K.; McMahon, P. L.; Islam, Z.; Yamamoto, Y.; Fisher, I. R. In-Plane Resistivity Anisotropy in an Underdoped Iron Arsenide Superconductor. *Science* **2010**, *329*, 824−826.
(12) In two-dimensional systems of interest, the C_6 group can be generated by the C_3 and C_2 subgroups. Since the nematic state retains C_2 symmetry, the distinctions between C_3 and C_6 symmetries become irrelevant, rendering them effectively equivalent in this context.
(13) Fernandes, R. M.; Venderbos, J. W. F. Nematicity with a twist: Rotational symmetry breaking in a moiré superlattice. *Science Advances* **2020**, *6*, No. eaba8834.
(14) Chakraborty, A. R.; Fernandes, R. M. Strain-tuned quantum criticality in electronic Potts-nematic systems. *Phys. Rev. B* **2023**, *107*, 195136.
(15) Xie, Y.; Hardy, A.; Paramekanti, A. Orbital selective order and Z_3 Potts nematicity from a non-Fermi liquid. *Phys. Rev. B* **2024**, *110*, 165158.
(16) Little, A.; Lee, C.; John, C.; Doyle, S.; Maniv, E.; Nair, N. L.; Chen, W.; Rees, D.; Venderbos, J. W.; Fernandes, R. M.; Analytis, J. G.; Orenstein, J. Three-state nematicity in the triangular lattice antiferromagnet $Fe_{1/3}NbS_2$. *Nat. Mater.* **2020**, *19*, 1062−1067.
(17) Feng, Z.; Lu, W.; Lu, T.; Liu, F.; Sheeran, J. R.; Ye, M.; Xia, J.; Kurumaji, T.; Ye, L. Nonvolatile Nematic Order Manipulated by Strain and Magnetic Field in a Layered Antiferromagnet. *arXiv Preprint*, arXiv:2507.05486, 2025.
(18) Kirstein, E.; Park, P.; Cho, W.; Batista, C. D.; Park, J.-G.; Crooker, S. A. Tunable chiral and nematic states in the triple-Q antiferromagnet $Co_{1/3}TaS_2$. *Nat. Commun.* **2026**, na DOI: 10.1038/s41467-026-68843-0.
(19) Nie, L.; et al. Charge-density-wave-driven electronic nematicity in a kagome superconductor. *Nature* **2022**, *604*, 59−64.
(20) Xu, Y.; Ni, Z.; Liu, Y.; Ortiz, B. R.; Deng, Q.; Wilson, S. D.; Yan, B.; Balents, L.; Wu, L. Three-state nematicity and magneto-optical Kerr effect in the charge density waves in kagome superconductors. *Nat. Phys.* **2022**, *18*, 1470−1475.
(21) Asaba, T.; et al. Evidence for an odd-parity nematic phase above the charge-density-wave transition in a kagome metal. *Nat. Phys.* **2024**, *20*, 40−46.
(22) Farhang, C.; Meier, W. R.; Lu, W.; Li, J.; Wu, Y.; Mozaffari, S.; Madhogaria, R. P.; Zhang, Y.; Mandrus, D.; Xia, J. Discovery of an intermediate nematic state in a bilayer kagome metal ScV_6Sn_6. *Nat. Commun.* **2025**, *16*, 7867.
(23) Hwangbo, K.; Rosenberg, E.; Cenker, J.; Jiang, Q.; Wen, H.; Xiao, D.; Chu, J.-H.; Xu, X. Strain tuning of vestigial three-state Potts nematicity in a correlated antiferromagnet. *Nat. Phys.* **2024**, *20*, 1888−1895.
(24) Ni, Z.; Antonenko, D. S.; Meese, W. J.; Tian, Q.; Huang, N.; Haglund, A. V.; Cothrine, M.; Mandrus, D. G.; Fernandes, R. M.; Venderbos, J. W.; Venderbos, J. W. F.; Liang, W. Signatures of Z_3 Vestigial Potts-nematic order in van der Waals antiferromagnets. *arXiv Preprint*, arXiv:2308.07249, 2023.
(25) Tan, Q.; Occhialini, C. A.; Gao, H.; Li, J.; Kitadai, H.; Comin, R.; Ling, X. Observation of three-state nematicity and domain evolution in atomically thin antiferromagnetic $NiPS_3$. *Nano Lett.* **2024**, *24*, 7166−7172.
(26) Taylor, B.; Steger, J.; Wold, A.; Kostiner, E. Preparation and properties of iron phosphorus triselenide, $FePSe_3$. *Inorg. Chem.* **1974**, *13*, 2719−2721.
(27) Wang, Q. H.; et al. The Magnetic Genome of Two-Dimensional van der Waals Materials. *ACS Nano* **2022**, *16*, 6960−7079.
(28) Cui, J.; Bostrom, E. V.; Ozerov, M.; Wu, F.; Jiang, Q.; Chu, J.-H.; Li, C.; Liu, F.; Xu, X.; Rubio, A.; Zhang, Q. Chirality selective magnon-phonon hybridization and magnon-induced chiral phonons in a layered zigzag antiferromagnet. *Nat. Commun.* **2023**, *14*, 3396.
(29) Haglund, A. *Thermal conductivity of MXY_3 magnetic layered trichalcogenides*. Ph.D. thesis, University of Tennessee, Knoxville, TN, 2019.
(30) Chen, L.; Teng, X.; Hu, D.; Ye, F.; Granroth, G. E.; Yi, M.; Chung, J.-H.; Birgeneau, R. J.; Dai, P. Thermal evolution of spin excitations in honeycomb Ising antiferromagnetic $FePSe_3$. *npj Quantum Materials* **2024**, *9*, 40.
(31) Wiedenmann, A.; Rossat-Mignod, J.; Louisy, A.; Brec, R.; Rouxel, J. Neutron diffraction study of the layered compounds $MnPSe_3$ and $FePSe_3$. *Solid State Commun.* **1981**, *40*, 1067−1072.
(32) Bhutani, A.; Zuo, J. L.; McAuliffe, R. D.; dela Cruz, C. R.; Shoemaker, D. P. Strong anisotropy in the mixed antiferromagnetic system $Mn_{1-x}Fe_xPSe_3$. *Phys. Rev. Mater.* **2020**, *4*, 034411.
(33) Mo, Z.; Li, C.; Zhang, W.; Liu, C.; Sun, Y.; Liu, R.; Lu, X. Cryogenic Digital Image Correlation as a Probe of Strain in Iron-Based Superconductors. *Chin. Phys. Lett.* **2024**, *41*, 107102.
(34) Toth, S.; Lake, B. Linear spin wave theory for single-Q incommensurate magnetic structures. *J. Phys.: Condens. Matter* **2015**, *27*, 166002.
(35) Lu, X.; Park, J. T.; Zhang, R.; Luo, H.; Nevidomskyy, A. H.; Si, Q.; Dai, P. Nematic spin correlations in the tetragonal state of uniaxial-strained $BaFe_{2-x}Ni_xAs_2$. *Science* **2014**, *345*, 657−660.
(36) Kim, M. G.; Fernandes, R. M.; Kreyssig, A.; Kim, J. W.; Thaler, A.; Bud'ko, S. L.; Canfield, P. C.; McQueeney, R. J.; Schmalian, J.; Goldman, A. I. Character of the structural and magnetic phase transitions in the parent and electron-doped $BaFe_2As_2$ compounds. *Phys. Rev. B* **2011**, *83*, 134522.
(37) Lu, X.; Tseng, K.-F.; Keller, T.; Zhang, W.; Hu, D.; Song, Y.; Man, H.; Park, J. T.; Luo, H.; Li, S.; Nevidomskyy, A. H.; Dai, P. Impact of uniaxial pressure on structural and magnetic phase transitions in electron-doped iron pnictides. *Phys. Rev. B* **2016**, *93*, 134519.
(38) Liu, P.; Klemm, M. L.; Tian, L.; Lu, X.; Song, Y.; Tam, D. W.; Schmalzl, K.; Park, J. T.; Li, Y.; Tan, G.; Su, Y.; Bourdarot, F.; Zhao, Y.; Lynn, J. W.; Birgeneau, R. J.; Dai, P. In-plane uniaxial pressure-induced out-of-plane antiferromagnetic moment and critical fluctuations in $BaFe_2As_2$. *Nat. Commun.* **2020**, *11*, 5728.
(39) Tam, D. W.; Wang, W.; Zhang, L.; Song, Y.; Zhang, R.; Carr, S. V.; Walker, H. C.; Perring, T. G.; Adroja, D. T.; Dai, P. Weaker nematic phase connected to the first order antiferromagnetic phase transition in $SrFe_2As_2$ compared to $BaFe_2As_2$. *Phys. Rev. B* **2019**, *99*, 134519.
(40) Liu, R.; Stone, M. B.; Gao, S.; Nakamura, M.; Kamazawa, K.; Krajewska, A.; Walker, H. C.; Cheng, P.; Yu, R.; Si, Q.; Dai, P.; Lu, X. Magnetic ground state of FeSe. *Nat. Commun.* **2025**, *16*, 5212.
(41) See the Supporting Information for additional data and analyses.
(42) Bewley, R.; Eccleston, R.; McEwen, K.; Hayden, S.; Dove, M.; Bennington, S.; Treadgold, J.; Coleman, R. MERLIN, a new high count rate spectrometer at ISIS. *Physica B: Condensed Matter* **2006**, *385*−*386*, 1029−1031.
(43) Lu, X.; Zhang, W.; Tseng, Y.; Liu, R.; Tao, Z.; Paris, E.; Liu, P.; Chen, T.; Strocov, V. N.; Song, Y.; Yu, R.; Si, Q.; Dai, P.; Schmitt, T. Spin-excitation anisotropy in the nematic state of detwinned FeSe. *Nat. Phys.* **2022**, *18*, 806−812.

https://doi.org/10.1021/acs.nanolett.5c06293
Nano Lett. XXXX, XXX, XXX−XXX

(44) Lane, H.; Mourigal, M. Thermally induced mimicry of quantum cluster excitations and implications for the magnetic transition in $FePSe_3$. *Phys. Rev. B* **2025**, *111*, 174446.

https://doi.org/10.1021/acs.nanolett.5c06293
Nano Lett. XXXX, XXX, XXX−XXX